JOURNAL OF VIROLOGY, July 2007, p. 7449–7462 Vol. 81, No. 14
0022-538X/07/$08.00+0 doi:10.1128/JVI.00238-07

Temporal Analysis of Andes Virus and Sin Nombre Virus Infections of Syrian Hamsters▽

Victoria Wahl-Jensen,[1] Jennifer Chapman,[2] Ludmila Asher,[2] Robert Fisher,[1] Michael Zimmerman,[3] Tom Larsen,[2] and Jay W. Hooper[1]*

Virology Division,[1] Pathology Division,[2] and Veterinary Medicine Division,[3] U.S. Army Medical Research Institute of Infectious Diseases, Fort Detrick, Maryland 21702

Received 5 February 2007/Accepted 23 April 2007

Andes virus (ANDV) and Sin Nombre virus (SNV) are rodent-borne hantaviruses that cause a highly lethal hemorrhagic fever in humans known as hantavirus pulmonary syndrome (HPS). There are no vaccines or specific drugs to prevent or treat HPS, and the pathogenesis is not understood. Syrian hamsters infected with ANDV, but not SNV, develop a highly lethal disease that closely resembles HPS in humans. Here, we performed a temporal pathogenesis study comparing ANDV and SNV infections in hamsters. SNV was nonpathogenic and viremia was not detected despite the fact that all animals were infected. ANDV was uniformly lethal with a mean time to death of 11 days. The first pathology detected was lymphocyte apoptosis starting on day 4. Animals were viremic and viral antigen was first observed in multiple organs by days 6 and 8, respectively. Levels of infectious virus in the blood increased 4 to 5 logs between days 6 and 8. Pulmonary edema was first detected ultrastructurally on day 6. Ultrastructural analysis of lung tissues revealed the presence of large inclusion bodies and substantial numbers of vacuoles within infected endothelial cells. Paraendothelial gaps were not observed, suggesting that fluid leakage was transcellular and directly attributable to infecting virus. Taken together, these data imply that HPS treatment strategies aimed at preventing virus replication and dissemination will have the greatest probability of success if administered before the viremic phase; however, because vascular leakage is associated with infected endothelial cells, a therapeutic strategy targeting viral replication might be effective even at later times (e.g., after disease onset).

Hantavirus pulmonary syndrome (HPS) was first recognized in North America in 1993 during an outbreak of unexplained illness that led to acute respiratory distress and death in nearly half of the patients. The etiological agent was soon found to be a hantavirus, and an epidemiological link was established with exposure to excreta from infected rodents. Since 1993, numerous hantaviruses have been isolated throughout the Americas (5). To date, there have been over 1,900 cases of HPS with an overall case fatality of approximately 40% (29, 39). Sin Nombre virus (SNV) was the first hantavirus linked to HPS and is the cause of the majority of North American HPS cases. Andes virus (ANDV) is the cause of the majority of South American HPS cases and is the only hantavirus for which there is compelling evidence of person-to-person transmission (17, 24, 30). The rapid onset of HPS, high case fatality, and absence of drugs or vaccines make this disease a significant health concern in regions of endemicity. The recent importation of an ANDV-like virus from Bolivia to British Columbia, Canada (31), further underscores the need for additional research into the pathogenesis of and development of medical countermeasures to these highly lethal viruses.

Hantaviruses represent a diverse group of viruses within a separate genus of the family *Bunyaviridae*. Members of this genus share morphological similarities with other bunyaviruses, including a pleomorphic size (70 to 210 nm) and a generally spherical particle appearance (9). Virions possess a host-derived lipid envelope that is studded with oligomers of the envelope glycoproteins. The genome of hantaviruses is tripartite, negative-sense, single-stranded RNA that encodes three structural proteins (35). The small RNA segment (S) encodes the nucleoprotein (N), the medium segment (M) encodes the G_N and G_C envelope glycoproteins (previously known as G1and G2), and the large segment (L) encodes the viral RNA-dependent RNA polymerase. Unlike members of the other four genera within the *Bunyaviridae* family, hantaviruses are not transmitted through an arthropod vector but rather maintain an apathogenic and persistent infection within their natural rodent reservoir species. Human infection is associated with HPS or hemorrhagic fever with renal syndrome (HFRS) (28). Vascular leakage and kidney dysfunction are associated with HFRS, while HPS-associated hantaviruses cause acute pulmonary edema (16, 44). Cardiac dysfunction has also been associated with HPS, and the term hantavirus cardiopulmonary syndrome has been used by some groups to alert clinicians to this disease characteristic. Acute thrombocytopenia and changes in vascular permeability are common features of both diseases, and either may include pulmonary or renal features.

Previously, we reported the discovery that ANDV is highly lethal to Syrian hamsters (12). The disease in hamsters closely resembled HPS in humans, i.e., the incubation time was approximately 10 days to 2 weeks, onset was rapid, the disease involved infection of endothelial cells, and the organ primarily affected was the lungs. Interestingly, SNV was highly infectious in the hamsters (2 PFU was sufficient to infect 50% of the hamsters) but did not cause disease. Here, we performed a

* Corresponding author. Mailing address: Virology Division, USAMRIID, Fort Detrick, MD 21702. Phone: (301) 619-4101. Fax: (301) 619-2439. E-mail: jay.hooper@amedd.army.mil.

▽ Published ahead of print on 2 May 2007.

pathogenesis study comparing ANDV and SNV infections in hamsters. Hamsters were injected with ANDV or SNV by the intramuscular route, and then on days 0, 2, 4, 6, 8, 10, 12, 14, 16, and 21, blood and other tissue samples were collected and full necropsies were performed. The pathology studies involved both immunohistological and electron microscopic evaluations of tissues collected at serial time points after infection.

MATERIALS AND METHODS

Viruses and cells. ANDV strain Chile-9717869 and SNV strain CC107 (34) were propagated in Vero E6 cells (Vero C1008; ATCC CRL 1586). Preparation of ANDV passage 2, twice-plaque-purified virus stocks was previously described (12). The same method was used to prepare a twice-plaque-purified stock of SNV. Passage 2 stocks of both ANDV and SNV were used in this study.

Intramuscular injection of hamsters with virus. Female Syrian hamsters weighing 150 to 200 g (Harlan, Indianapolis, IN) were anesthetized by an intramuscular injection with approximately 0.1 ml/100 g of body weight of a ketamine-acepromazine-xylazine mixture. Once anesthetized, hamsters were injected intramuscularly (caudal thigh) with 0.2 ml of virus (2,000 PFU) diluted in phosphate-buffered saline, pH 7.4. After viral challenge, hamsters were placed in isolator units (one to four hamsters per cage). All work involving hamsters infected with ANDV or SNV was performed in a biosafety level 4 (BSL-4) laboratory. Hamsters were observed two to three times daily.

ELISA. There is a high degree of immune serum cross-reactivity to the nucleocapsid proteins of ANDV, SNV, and Puumala virus. This cross-reactivity made it possible to use the Puumala virus nucleocapsid-based enzyme-linked immunosorbent assay (ELISA) for detecting antibodies to ANDV and SNV nucleocapsid. Anti-nucleocapsid antibody ELISAs were performed as previously described (11). The plasmid pPUUSXdelta (kindly provided by F. Elgh) was expressed in *Escherichia coli* BL21(DE3) cells (Novagen, Madison, WI) to generate histidine-tagged truncated Puumala virus nucleocapsid fusion protein. The fusion protein was subsequently affinity purified in Ni-nitrilotriacetic acid columns (QIAGEN, Valencia, CA). Samples were gamma irradiated (on dry ice) with 3×10^6 rads from a ^{60}C source.

PRNT. Plaque reduction neutralization tests (PRNT) were performed as previously described (12). Samples were gamma irradiated as described above.

Blood chemistry. Serum samples were obtained from animals and gamma irradiated as described above. Concentrations of albumin, alkaline phosphatase, alanine aminotransferase, amylase, aspartate aminotransferase, total bilirubin, urea nitrogen, calcium, cholesterol, creatinine, glucose, and total protein were determined using a general chemistry 12-disc panel rotor and a Piccolo point-of-care blood analyzer (Abaxis, Sunnyvale, CA).

Hematology. Blood samples were collected in Safe-T-Fill capillary blood collection tubes containing EDTA (RAM Scientific, Yonkers, NY). Total white blood cell count, white blood cell differential count, red blood cell count, hemoglobin concentration, hematocrit, mean corpuscular volume, mean corpuscular hemoglobin, mean corpuscular hemoglobin concentration, and platelet count were determined from blood samples collected in EDTA by using an A^c T 10 Coulter Counter (Coulter Electronics, Hialeah, FL). In addition, blood smears were prepared and manual counts were obtained by standard methods. Data were analyzed using the Wilcoxon rank-sum test.

Preparation of tissue for histology. Tissues (lung, liver, spleen, heart, thymus, trachea, thyroid gland, gastrointestinal tract, pancreas, kidneys, adrenal glands, urinary bladder, uterus, ovaries, skin, submandibular salivary gland, multiple lymph nodes, brain, pituitary gland, eyes, and nasal turbinates) were fixed in 10% neutral buffered formalin, trimmed, processed, embedded in paraffin, cut at 5 to 6 μm, and stained with hematoxylin & eosin (H&E) according to established protocols (32). Immunolocalization of ANDV and SNV in tissues was performed with an alkaline phosphatase procedure (EnVision System; DAKO Corp., Carpinteria, CA) or an immunoperoxidase procedure (horseradish peroxidase EnVision System; DAKO) according to the manufacturer's directions. The primary antibody was an anti-SNV nucleocapsid rabbit polyclonal diluted 1:500 for the alkaline phosphatase procedure or 1:3,000 for the peroxidase procedure (provided by Diagnostic Service Division, USAMRIID). Negative controls included naïve hamster tissue incubated with nonimmune rabbit immunoglobulin G in place of the primary antibody and naïve hamster tissue exposed to the primary antibody and to negative serum. Tissue sections were pretreated in proteinase K for 6 min (DAKO) at room temperature and blocked with CAS-BLOCK (Invitrogen, Carlsbad, CA) and 5% goat serum (Vector Laboratories, Burlingame, CA) for 30 min at room temperature. The primary antibody was incubated on the tissue sections for 1 h at room temperature for the alkaline phosphatase procedure or for 30 min at room temperature for the peroxidase procedure. Goat anti-rabbit antibodies conjugated to an alkaline phosphatase-labeled dextran polymer or horseradish peroxidase-labeled dextran polymer provided with the EnVision kit served as the secondary antibody for that system. The secondary antibody was incubated for 30 min at room temperature. Sections were incubated for 6 min with the DakoCytomation Permanent Red substrate-chromogen system or 5 min with 3,3′-diaminobenzidine (DAKO). Immunostained sections were counterstained with hematoxylin and dehydrated, and coverslips were applied with Permount (Fisher Scientific).

Electron microscopy. Lungs, liver, heart, spleen, and kidneys were analyzed by transmission electron microscopy by fixing tissues for 24 h with 4% paraformaldehyde and 1% glutaraldehyde, treated with 1% osmium tetroxide for 1 h, washed, en block stained with 0.5% uranyl acetate, dehydrated in graded ethanol and propylene oxide, and embedded in PolyBed 812 (Polysciences, Warrington, PA). Ultrathin sections were stained with uranyl acetate and lead citrate and examined at 80 kV on a JOEL 1011 transmission electron microscope.

Tissue samples for immunoelectron microscopy were fixed for 1 month in 2% paraformaldehyde and 0.1% glutaraldehyde, dehydrated through graded ethanols up to 70%, and embedded in LR White resin (Polysciences, Warrington, PA). Ultrathin sections were placed on nickel grids and prepared for immunoelectron microscopy by an indirect method. The primary antibody was a rabbit anti-SNV nucleocapsid polyclonal antibody (see above) diluted 1:300. The secondary antibody was a goat anti-rabbit serum labeled with 10-nm gold particles (Ted Pella Inc., Redding, CA) and diluted 1:30. As a negative control, sections from the same block were incubated with normal rabbit serum (Vector Laboratories, Burlingame, CA) at the same dilution as the primary serum. Grids were first floated on the blocking serum, in this case normal goat serum (Vector Laboratories, Burlingame, CA), for 20 min at room temperature and then on the primary serum for 1 h at room temperature or overnight at 4°C. After rinsing grids in BTT buffer (20 mM Tris, 0.9% NaCl, 0.1% bovine serum albumin, and 0.5% Tween), sections were incubated with the secondary antibody for 1 h, rinsed again, and fixed in 1% glutaraldehyde for 5 min. Grids were stained with uranyl acetate and lead citrate and examined on a JOEL 1011 microscope.

Plaque assay. Hantavirus plaque assays were performed as previously described (12). Briefly, serum samples were centrifuged to pellet any debris before dilution. Whole blood collected in K_2EDTA tubes was transferred to centrifuge tubes, rapidly freeze-thawed three times, and then spun in a microcentrifuge at $10{,}000 \times g$ for 10 s to pellet debris. Supernatants were used to prepare initial dilutions. Similarly, throat swabs were processed by first adding 300 μl of Eagle's minimal essential medium with Earl's salts containing 10% fetal bovine serum, 10 mM HEPES (pH 7.4), penicillin (100 U/ml), streptomycin (100 μg/ml), and gentamycin sulfate (50 μg/ml) to swabs in microcentrifuge tubes for 3 min. Swabs were then swirled to release sample material into the medium. The throat swab suspension was then freeze-thawed three times and spun in a microcentrifuge at $10{,}000 \times g$ for 10 s. Supernatants were used to prepare dilutions starting at 1:10. Once sample dilutions were prepared, 200 μl was added to each well of a six-well Costar plate containing 7-day-old Vero E6 monolayers. After a 1-h adsorption at 37°C, 3 ml of overlay medium was added to each well as previously described (12). Plates were incubated at 37°C in a humidified 5% CO_2 environment for 7 days. Plaques were stained on day 7 (ANDV) or day 10 (SNV) by adding 2 ml/well of overlay medium containing 5% fetal bovine serum and 5% neutral red solution (Invitrogen, Carlsbad, CA). Plates were then incubated for an additional 2 days at 37°C or until plaques were visible and countable.

Isolation of PBMCs and real-time PCR. Peripheral blood mononuclear cells (PBMCs) were isolated by adding 1 ml ACK lysing buffer (BioSource, Camarillo, CA) to 200 μl EDTA blood, gently mixed by inversion, incubated for 5 min at room temperature, and then centrifuged at $1{,}500 \times g$ for 5 min. Supernatants were discarded and the cell pellet was resuspended in 1 ml phosphate-buffered saline. Samples were centrifuged at $1{,}500 \times g$ for 5 min. Supernatants were discarded and the cell pellet was resuspended in 1 ml of TRIzol (Invitrogen, Carlsbad, CA) and mixed by pipetting. RNA was extracted from TRIzol samples as recommended by the manufacturer. Reverse transcriptase (RT) and real-time PCRs were performed as previously described (25). Briefly, 10 ng of RNA was used for the RT reaction using a primer specific for the negative-sense strands of the ANDV and SNV S-segments. The RT primers were as follows: ANDV S 350F (5′CATCTC TGA GAT ATG GGA ATG TCC TGG-3′) and SNV S 10F (5′-ACT CCT TGA GAA GCT ACT ACG AC-3′). A 2.5-μl portion of cDNA generated from the RT reaction was used in the real-time PCR, which was performed as previously described with ANDV-S- and SNV-S-specific primers and probes (26).

RESULTS

Study design. We previously reported that ANDV was highly lethal in hamsters, whereas SNV was highly infectious but did not cause disease (12). Moreover, we reported that a reassortant virus having an ANDV M genome segment and SNV S and L genome segments was infectious in hamsters but did not cause disease (26). Here we performed a serial pathogenesis study to (i) determine when and to what tissues and cell types ANDV and SNV disseminate after challenge, (ii) measure and evaluate hematological changes during the course of ANDV and SNV infections, (iii) determine if blood chemistries in ANDV- or SNV-infected hamsters reveal evidence of organ dysfunction, and (iv) use immunohistochemical techniques and electron microscopy to characterize the inflammation and ultrastructural changes in tissues of hamsters with HPS.

The study consisted of animals in time course groups (8 hamsters injected with ANDV and 8 hamsters injected with SNV) and animals in serial pathology groups (24 hamsters injected with ANDV and 24 hamsters injected with SNV). Animals in the time course groups were weighed, throat swabbed, and bled 1 week before challenge, at the time of challenge, and then every 2 days until day 16. This time course group-based data collection method allowed us to collect samples from the same hamster over time throughout the experiment. Animals in the serial pathology groups were weighed and bled 1 week before challenge and assigned predetermined necropsy dates. On the day of challenge and every 2 days thereafter for 16 days, three ANDV-injected hamsters and three SNV-injected hamsters were removed from the serial pathology groups, and full necropsies were performed (including blood collections and throat swabs for viremia study). In some cases, moribund animals from the time course group were euthanized and necropsies were performed. This was done to ensure that at least three hamsters were necropsied at each of the time points. The fates of the individual animals in each group are shown in Table 1.

TABLE 1. Study design

Group	Hamster ID no.[a]	Fate[b]	Day	Necropsy
ANDV time course	201	FD	13	
	202	FD*	7	
	203	FD	11	
	204	FD	11	
	205	SAC	14	Yes
	206	EUTH	12	Yes
	207	SAC	14	Yes
	208	FD	11	
SNV time course	209			
	210	Survived		
	211	Survived		
	212	Survived		
	213	Survived		
	214	Survived		
	215	Survived		
	216	Survived		
ANDV serial pathology	217	SAC	2	Yes
	218	SAC	2	Yes
	219	SAC	2	Yes
	220	SAC	4	Yes
	221	SAC	4	Yes
	222	SAC	4	Yes
	223	SAC	6	Yes
	224	SAC	6	Yes
	225	SAC	6	Yes
	226	SAC	8	Yes
	227	SAC	8	Yes
	228	SAC	8	Yes
	229	SAC	10	Yes
	230	SAC	10	Yes
	231	SAC	10	Yes
	232	FD	10	
	233	SAC	12	Yes
	234	FD	14	
	235	FD	10	
	236	FD	11	
	237	EUTH	10	
	238	EUTH	12	Yes
	239	SAC	14	Yes
	240	EUTH	10	
SNV serial pathology	241	SAC	2	Yes
	242	SAC	2	Yes
	243	SAC	2	Yes
	244	SAC	4	Yes
	245	FD*	−7	Yes
	246	SAC	4	Yes
	247	SAC	6	Yes
	248	SAC	6	Yes
	249	SAC	6	Yes
	250	SAC	8	Yes
	251	SAC	8	Yes
	252	SAC	8	Yes
	253	SAC	10	Yes
	254	SAC	10	Yes
	255	SAC	10	Yes
	256	SAC	12	Yes
	257	SAC	12	Yes
	258	SAC	12	Yes
	259	SAC	14	Yes
	260	SAC	14	Yes
	261	SAC	14	Yes
	262	SAC	16	Yes
	263	SAC	16	Yes
	264	SAC	16	Yes
No challenge	265	SAC	−7	Yes
	266	SAC	−7	Yes
	267	SAC	−7	Yes

[a] ID, identification.
[b] FD, found dead; FD*, suspect death due to blood draw; SAC, no signs of disease when sacrificed; EUTH, moribund animal euthanized.

Clinical signs and hematological analysis. The hamsters infected with ANDV were either found dead, found moribund and euthanized, or killed for necropsy on the indicated day (Table 1). Across all groups, there were 14 hamsters that were found dead or were found moribund and euthanized. Two hamsters were suspected to have died due to the blood draw procedure, one on day −7 and one on day 7, and were not included in further analysis. Of the remaining 12 hamsters, all had been injected with ANDV, and the mean time to death was 11 days. None of the SNV-injected hamsters displayed signs of disease, and all survived or were killed for scheduled necropsies. Nevertheless, all of the hamsters injected with SNV were indeed infected because they had anti-nucleocapsid antibody titers as measured by ELISA. ELISA endpoint titers on sera collected on day 28 (terminal bleed) ranged from 200 to 6,400, with a geometric mean titer of 872. All sera collected before day 16 were negative by ELISA. Three of the day 28 sera were further evaluated for neutralizing antibody by PRNT. All were positive, with 80% PRNT titers of 320, 160, and >640. ANDV-injected animals displayed obvious signs of illness within a few hours before death. Signs included tachypnea, staggered gait, cyanosis (bluing of nares and oral cavity), and apparent weakness. There was minor (<6%) weight loss in the ANDV-injected hamsters during the 2 days before death (data not shown).

Blood samples collected from the animals in the serial pathology groups were analyzed by Coulter Counter and manual differential analysis (smears). ANDV-injected animals exhibited an absolute increase in white blood cell counts that was

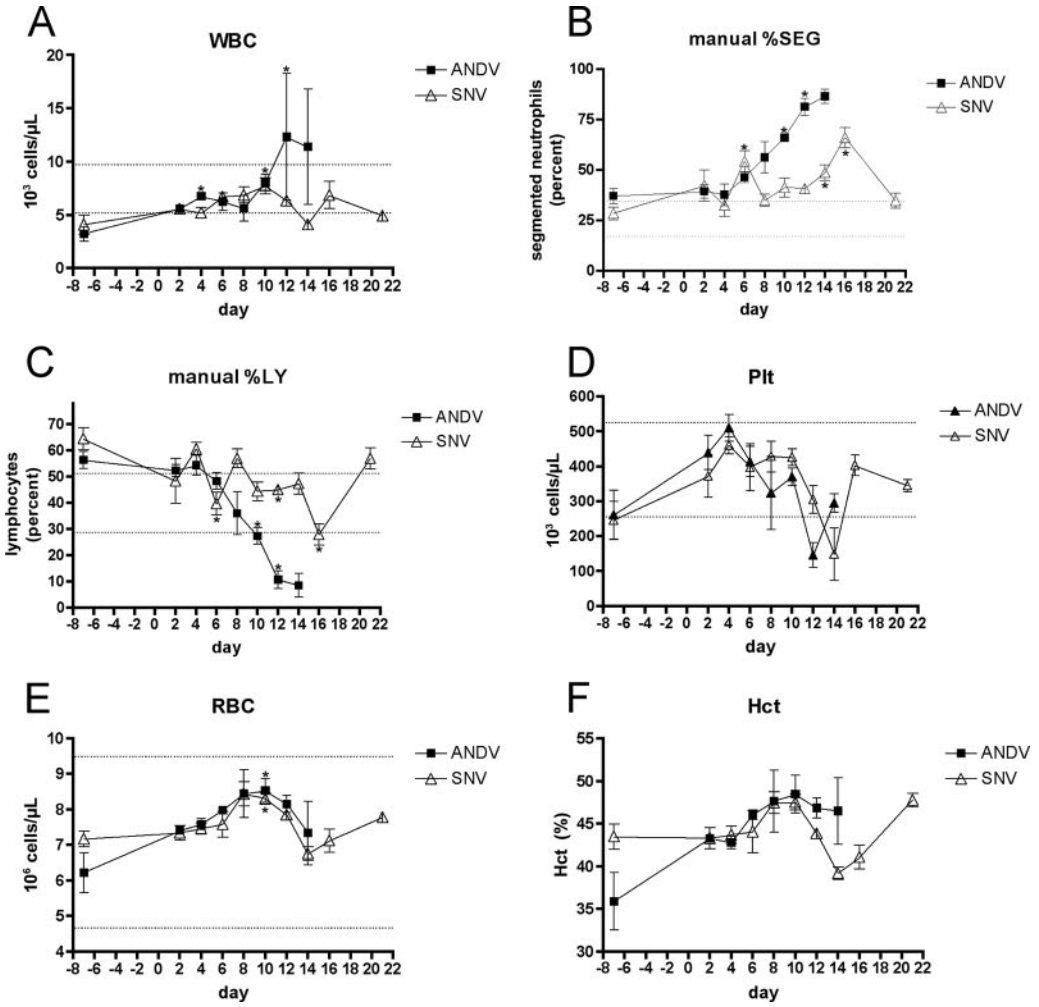

FIG. 1. Hematological findings. ANDV and SNV serial pathogenesis groups were analyzed for changes in hematological parameters after infection. The area between dotted lines represents the normal reference range for hamsters. ANDV-infected animals exhibited white blood cell (WBC) counts above normal reference values (A) with a corresponding increase in the percent segmented neutrophils (%SEG) beginning on day 10 (B). (C and D) Lymphopenia (%LY) and thrombocytopenia (Plt) were also observed with ANDV infection, although similar changes were also observed with SNV that occurred later and to a lesser degree. (E and F) Slight rises in red blood cell (RBC) and hematocrit (Hct) were also observed with ANDV and SNV but remained within normal limits. Symbols represent the mean values for each time point. Error bars represent the standard errors of the means (SEM). Asterisks represent statistically significant ($P < 0.05$) differences relative to day −7 values.

outside of normal reference values (Fig. 1). This was likely due to a relative neutrophilia with a peak in segmented neutrophils occurring at the terminal stages of disease (days 12 to 14). We did not observe a significant increase in the percentage of banded neutrophils (data not shown). Interestingly, there was a delayed neutrophilia with SNV, but the increase in segmented neutrophils was not as pronounced as what was seen with ANDV. A relative lymphopenia that was outside normal limits was seen with ANDV on days 12 to 14. Finally, transient thrombocytopenia was observed for both ANDV- and SNV-infected animals, peaking at days 12 and 14, respectively. The small sample size detracted from our ability to assign statistical significance (Wilcoxon rank-sum test) to the observed postinfection alterations in hematological values. A comparison of the ANDV and SNV data for each time point indicated that there were no statistically significant differences between those groups; however, there were significant changes from the prechallenge values (Fig. 1).

Viremia is not detected in SNV-infected hamsters. We previously reported that serum viremia (infectious virus) in hamsters injected with ANDV could be detected on day 8 postinfection (12). Here, we included additional time points to gain further insight into the kinetics of ANDV viremia in the hamster model. In addition, we assayed for the presence of viremia in hamsters injected with SNV. Plaque assays were used to measure infectious virus in whole blood and in serum from the animals in the serial pathology groups. ANDV was first detected in whole blood and serum on day 6 postinfection and peaked by days 8 and 12 postinfection, respectively (Fig. 2A and B). In stark contrast, infectious SNV was not detected in the serum or whole blood at any time point. It was possible that SNV virions had disseminated into the blood but were ren-

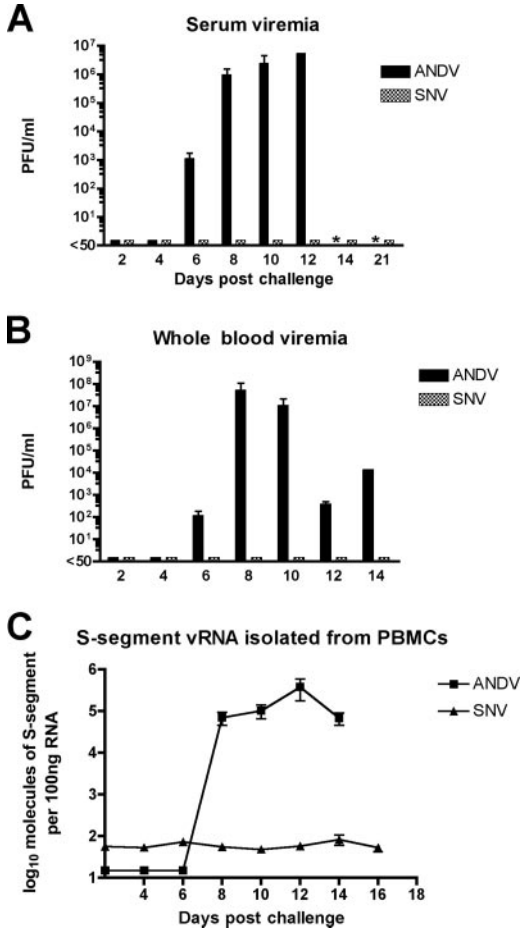

FIG. 2. Kinetics of viremia. Hantavirus plaque assays were performed on serum (A) and whole blood (B) collected from ANDV- and SNV-infected hamsters. The limit of detection was 50 PFU/ml. (C) RNA was isolated from PBMCs, and real-time PCR was performed following cDNA synthesis. Samples were analyzed for the presence of S-segment viral RNA (vRNA). Levels of SNV nucleocapsid did not rise above background levels, indicating that SNV did not productively infect these cells. All data shown represent the average values for all animals within each group ($n = 3$). Error bars represent the SEM. Asterisks indicate samples not available for testing.

dered noninfectious (e.g., neutralized by innate immune responses such as complement). To investigate the possibility that noninfectious SNV was present in the blood, we performed real-time PCR to detect viral genomes in PBMCs collected on the days after challenge with ANDV or SNV (Fig. 2C). ANDV genomes were first detected on day 8 and were detected on all other time points until death. SNV genomes were not detected at any time point. Thus, either SNV did not enter the bloodstream or the numbers of circulating virions were exceedingly low (7 logs lower than the peak level of infectious ANDV in the days preceding disease onset). In addition to looking at viremia in the blood, we performed plaque assays on throat swab samples collected during the course of the study. No infectious ANDV or SNV was detected in throat swab samples at any time point (limit of detection was 50 PFU/ml). For ANDV-infected hamsters, this was unexpected because there were >5 logs of virus per ml of serum on days 8 to 12 postchallenge, and large volumes of fluid, presumably plasma, passed into the alveolar spaces (pulmonary edema) at the later time points.

Low level of SNV dissemination occurs despite undetectable viremia. The finding that SNV was not present in the blood and yet was highly infectious, as measured by seroconversion (50% infective dose is 2 PFU [12]), led us to look for virus in the major organs typically associated with hantavirus infection, including the lungs, liver, spleen, and kidneys. Both postmortem and histological examination indicated that these organs had no significant inflammation or other lesions. Immunohistological examination revealed SNV antigen, albeit rarely, in cells of endothelial origin in multiple organs on days 12 and 14 postinfection (Fig. 3). Thus, SNV was not found in the blood of infected hamsters but was occasionally found in endothelial cells in the lungs, heart, kidney, and brain. This low level of infectivity was capable of eliciting a robust immune response but no overt disease.

Temporal pathology following injection of ANDV or SNV. (i) Gross examination. To characterize the temporal pathology associated with ANDV or SNV infection, cohorts of 24 hamsters were injected with either ANDV or SNV, and then on days 0, 2, 4, 6, 8, 10, 12, and 14, three hamsters were euthanized and full necropsies were performed. Because of the number of ANDV-injected animals found dead after day 10, hamsters from the time course group were used to bring the number of necropsied animals to three per time point on days 12 and 14 (Table 1). Any animal found moribund was euthanized. Postmortem examination of ANDV-infected hamsters revealed large volumes of yellow or red effusion in the thoracic cavities of animals that succumbed to infection on day 12 (three of three animals [233, 206, and 238]) or 14 (two of three animals [239 and 207]), as previously reported (12). Large volumes of pleural effusion were not observed on any of the days preceding day 12, although there were small volumes of effusion in some animals as early as day 2 postinfection. One day 14 animal (205) was not viremic and did not have gross lesions consistent with viral infection.

(ii) Immunohistochemistry. Immunohistochemistry was performed on all organs examined histologically by H&E staining. Viral antigen was detected in the endothelial cells of multiple organs and hepatocytes in ANDV-infected hamsters starting on day 8 postinfection (Table 2). There was also rare immunoreactivity in the urothelium of the urinary bladder (one day 12 animal [206] and two day 14 animals [207 and 239]), the olfactory epithelium (one day 12 animal [206]), and the squamous epithelium lining the nonglandular stomach (one day 12 animal [206]) of ANDV-infected hamsters (data not shown). SNV-infected animals on day 12 (two of three animals [256 and 258]) and 14 (three of three animals [259, 260, and 261]) had very rare, scattered immunoreactivity in endothelial cells in multiple organs (kidney, heart, lungs, and brain) as described above. This pattern was so infrequent that as few as one cell to a maximum of only several cells in the entire tissue examined were immunoreactive (Fig. 3). Interestingly, one day 14 ANDV-infected animal (animal 205) did not develop viremia but had similar rare immunoreactivities in endothelial cells in multiple organs (data not shown).

Pathology in the lungs. The lungs from ANDV-infected hamsters appeared normal through day 6. Mild changes, in-

TABLE 2. Summary of temporal histopathological findings

Day postchallenge	Virus	Hamster ID no.[a]	Temporal histopathological finding[b]							
			Lung				Liver			Spleen mononuclear infiltrate
			IHC	Alveolar edema	Interstitial inflammation	Perivascular/ peribronchial inflammation	IHC	Hepatitis	Hepatocellular necrosis	
−7	None	265	−	−	−	−	−	−	−	−
	None	266	−	−	−	−	−	−	−	−
	None	267	−	−	−	−	−	−	−	−
2	ANDV	217	−	−	−	−	−	−	−	−
	ANDV	218	−	−	−	−	−	−	−	−
	ANDV	219	−	−	−	−	−	−	−	−
4	ANDV	220	−	−	−	−	−	−	−	−
	ANDV	221	−	−	−	−	−	−	−	−
	ANDV	222	−	−	−	−	−	−	−	−
6	ANDV	223	−	−	−	−	−	−	−	−
	ANDV	224	−	−	−	−	−	−	−	−
	ANDV	225	−	−	−	−	−	−	−	−
8	ANDV	226	+	+++	++	+++	+	+++++	++++	−
	ANDV	227	+	−	+	++	+	−	−	−
	ANDV	228	−	−	++	++	−	++	−	−
10	ANDV	229	++	++	++	++	+++	++	−	−
	ANDV	230	+++	−	++	−	+++	−	−	−
	ANDV	231	++	−	++	+++	++	+++++	+++++	−
12	ANDV	233	+++	−	+++	++++	+++	++	+++	−
	ANDV	238	+++	+++++	+++++	++++	+++	++	++	−
	ANDV	206	+++	++	+++	++	+++	+++	+++++	+++++
14	ANDV	239	+++	+++++	+++++	+++++	++	++	++	−
	ANDV	205	*	−	−	++	*	−	−	−
	ANDV	207	+++	−	++	++	+++	++++	++++	+++++
2	SNV	241	−	−	−	−	−	−	−	−
	SNV	242	−	−	−	−	−	−	−	−
	SNV	243	−	−	−	−	−	−	−	−
4	SNV	244	−	−	−	−	−	−	−	−
	SNV	246	−	−	−	−	−	−	−	−
6	SNV	247	−	−	−	−	−	−	++	−
	SNV	248	−	−	−	−	−	−	−	−
	SNV	249	−	−	−	−	−	+++	−	−
8	SNV	250	−	−	−	−	−	−	−	−
	SNV	251	−	−	−	−	−	−	−	−
	SNV	252	−	−	−	−	−	−	−	−
10	SNV	253	−	−	−	−	−	++	−	−
	SNV	254	−	−	−	−	−	++	−	−
	SNV	255	−	−	−	−	−	++	++	−
12	SNV	256	*	−	−	−	*	−	−	−
	SNV	257	−	−	−	−	−	−	−	−
	SNV	258	*	−	−	−	*	−	−	−
14	SNV	259	*	−	−	++	*	−	−	−
	SNV	260	*	−	−	++	*	−	−	−
	SNV	261	*	−	−	−	*	−	−	−
16	SNV	262	−	−	−	−	−	−	−	−
	SNV	263	−	−	−	++	−	−	−	−
	SNV	264	−	−	−	−	−	−	−	−
28	SNV	210	−	−	−	−	−	−	−	−
	SNV	213	−	−	−	−	−	−	−	−
	SNV	215	−	−	−	−	−	−	−	−

[a] ID, identification.

[b] IHC, immunohistochemistry. Immunostaining was scored from + to +++ (minimal to maximal staining, respectively). *, Scattered rare endothelial cell immunoreactivity; −, no immunostaining. Histopathological findings were scored as follows: +, very mild; ++, mild; +++, moderate; ++++, marked; +++++, severe. *, Scattered rare histopathology; −, negative or minimal finding.

cluding thickening of alveolar septal walls, were first observed on day 8 (Table 2). The damage to the lungs increased over time and culminated with severe pulmonary edema, mononuclear cell infiltration, and hemorrhage by day 14. Representative images are shown in Fig. 4. The inflammatory component consisted primarily of lymphocytes, plasma cells, and fewer neutrophils that expanded the alveolar, perivascular, and peribronchiolar interstitia. H&E-stained lungs from SNV-infected hamsters were unremarkable at all time points and resembled the lungs of the negative control animals (data not shown).

The most striking ultrastructural changes were seen in the lungs. The first signs of focal pulmonary edema were noticed

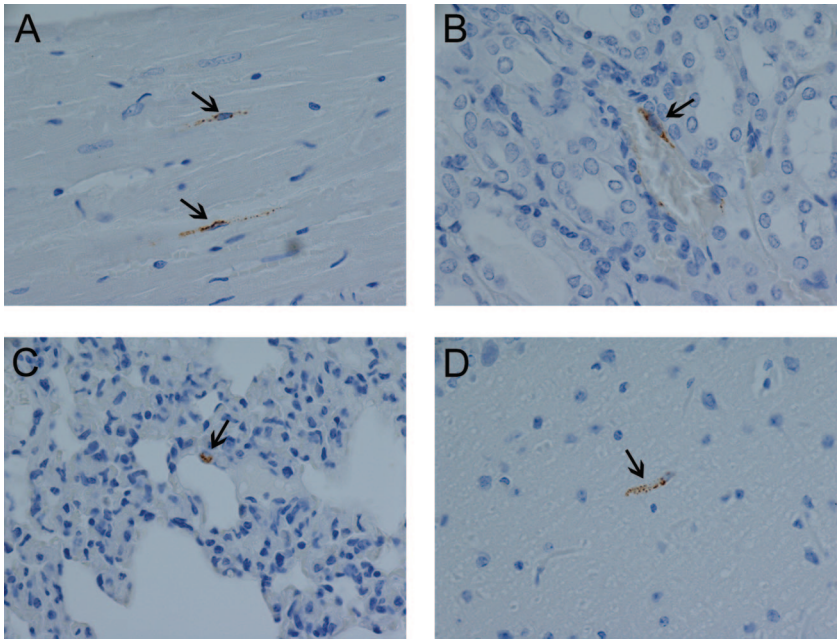

FIG. 3. Immunohistochemistry of SNV-infected hamsters. An immunoperoxidase-based immunohistochemical assay using anti-nucleocapsid antibody was performed on tissues from SNV-infected animals (Table 2). Immunopositive cells (presumably endothelial cells) were found rarely in multiple organs of SNV-infected hamsters at late times during infection (day 14). Only individual antigen-positive cells were observed, while ubiquitous endothelial cell staining was observed with ANDV. Representative samples include heart of animal 260 (A), kidney of animal 260 (B), lung of animal 260 (C), and brain of animal 261 (D). All images were acquired at a magnification of ×60. Arrows are shown in all images to highlight antigen-positive cells.

at day 6. No significant changes in alveolar epithelial cells or capillary endothelial cells were detected at that time. By day 8, alveolar edema became diffuse and was often accompanied by fibrin precipitation and an accumulation of extracellular surfactant (Fig. 5A). Some endothelial cells contained granular and granulofilamentous inclusions (Fig. 5B and C), which is typical for hantavirus infection, as early as day 8. The number and size of these inclusions increased with time. Similar inclusions were found in endothelial cells of kidneys, spleen, heart, and liver (data not shown; also see Fig. 7). Intracellular edema of type 1 pneumocytes with disruption of cellular membranes and thinning of the basement membranes was also frequently observed starting on day 8 (Fig. 5D and E). Starting on day 4, apoptotic lymphocytes (Fig. 5F) and, less frequently, polymorphonuclear leukocytes (data not shown) were observed in lung capillaries. The numbers of apoptotic lymphocytes and polymorphonuclear leukocytes increased with time.

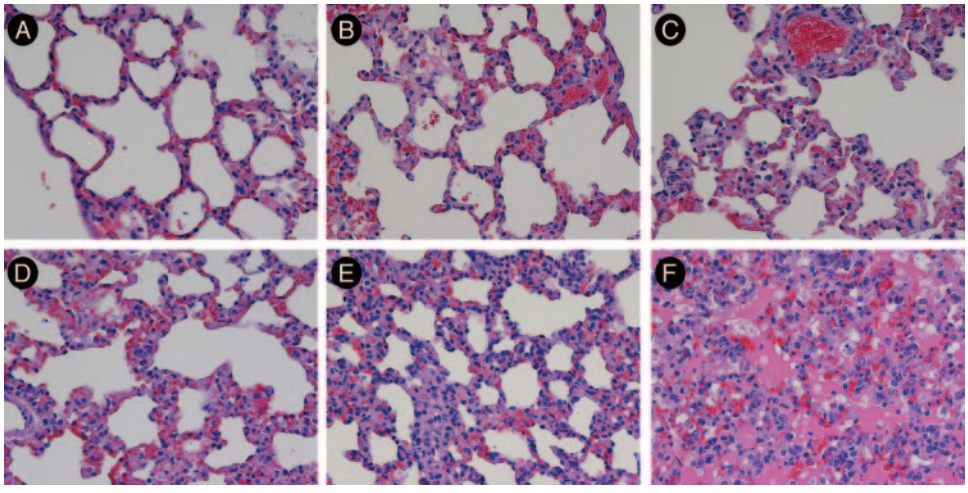

FIG. 4. Lung pathology in ANDV-infected hamsters. H&E staining of lungs collected from normal hamsters (day −7) (266) (A) or from ANDV-infected hamsters on day 4 (222), 6 (225), 8 (228), 12 (233), or 14 (239) (B to F, respectively). H&E-stained tissue is shown. Size bars = 50 μm. Note the temporal increase in septal wall thickening and filling of alveolar spaces with edema, fibrin, and inflammatory cells.

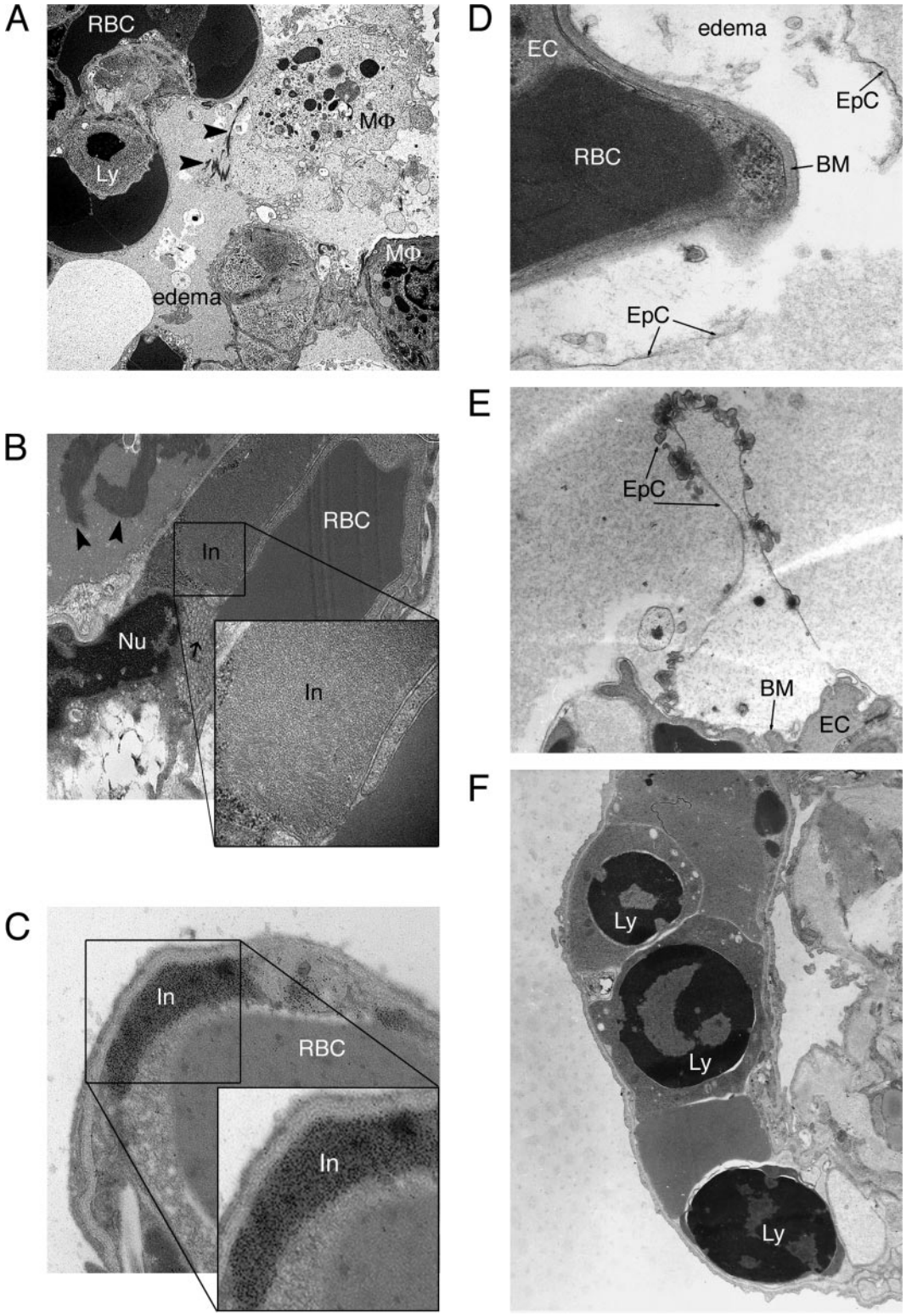

FIG. 5. Ultrastructural changes to ANDV-infected hamster lungs. Thin-section transmission electron microscopy was performed on ANDV-infected hamster lungs. (A) Fibrin deposition (arrowheads), alveolar airspace edema, and apoptotic lymphocytes were observed for animal 226 at 8 days postchallenge. Original magnification, ×40,000. (B) At day 12 postchallenge (animal 206), fibrin deposition was increased (arrowheads), and large granulofilamentous inclusions that occupied the majority of space in the endothelial cell cytoplasm could be observed. Numerous vacuoles were often observed in the endothelial cell cytoplasm, adjacent to the large inclusion (arrow). The inclusions were highly structured, as shown in the enlarged inset. Original magnifications, ×15,000 and ×80,000 (inset). (C) Endothelial cell inclusions were of viral origin, as demonstrated by immunoelectron microscopy using an anti-nucleocapsid antibody and a secondary antibody conjugated to 10-nm gold particles. The immunoreactive endothelial cell inclusion is enlarged for better visualization of gold particles (inset). Original magnifications, ×40,000 and ×80,000 (inset).

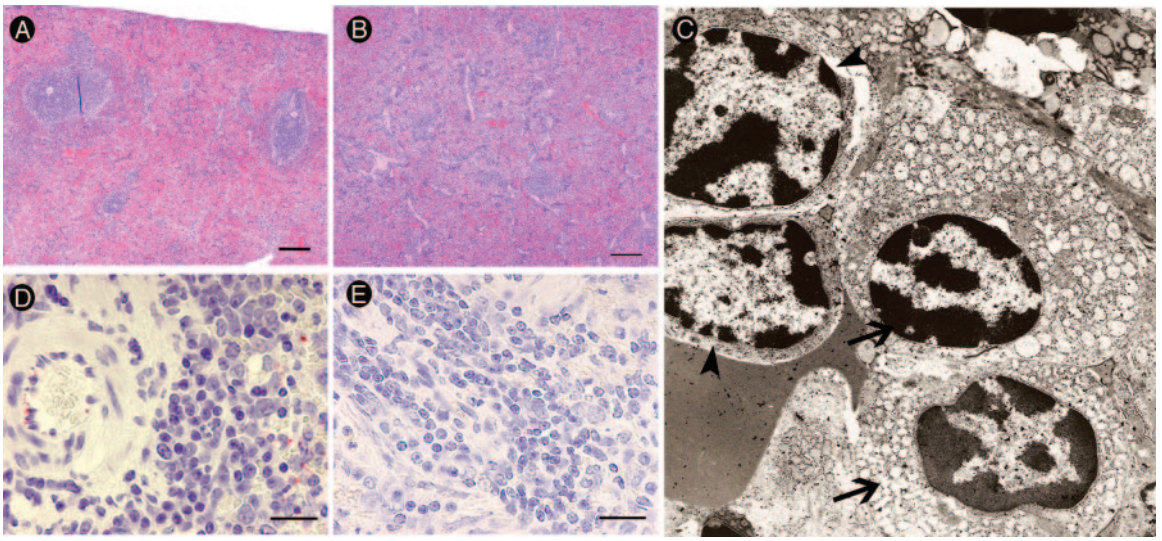

FIG. 6. Mononuclear cell infiltrate of the spleen. Mononuclear infiltrate was noted in the spleens of some ANDV-infected animals. (A) Normal appearance of spleen from an SNV-injected hamster (animal 265, day −7). (B) Mononuclear cell infiltrate in the red pulp that obscures lymphoid follicular architecture in splenic white pulp from an ANDV-infected hamster (animal 206, day 12). (C) Lymphoblasts (arrowhead) and plasma cells (arrows) are the predominant cell types associated with the mononuclear infiltrate, as shown by electron microscopy (animal 206, day 12). (D and E) Immunohistochemistry reveals viral antigen present in endothelial cells randomly scattered throughout the spleens from ANDV-infected hamsters (D) but not control hamsters (E). Size bars = 200 μm (A and B) and 20 μm (D and E). The electron microscopy image in panel C was acquired at a magnification of ×13,500.

Pathology in the spleen. The spleens of two ANDV-infected animals (one day 12 animal [206] and one day 14 animal [207]) (Table 2) had a diffuse mononuclear cell infiltrate that expanded the splenic red pulp and obscured lymphoid architecture compared to what was seen for control and SNV-infected animals (Fig. 6A and B). The spleen was evaluated by electron microscopy, and the majority of these cells were identified as plasma cells and lymphoblasts (Fig. 6C). ANDV antigen was detected in the spleens of infected but not control animals (Fig. 6D and E).

Pathology in the liver. Changes in the liver ranged from mild to moderate hepatitis and hepatocellular necrosis in ANDV-infected hamsters, also beginning on day 8 postinfection and remaining static through the endpoint of the study (day 14) (Table 2). Immunohistochemistry revealed antigen in endothelial cells and hepatocytes in the livers from ANDV- but not SNV-infected hamsters starting on day 8 (Fig. 7A and B). The inflammatory component in the liver was distributed both periportally and randomly and was composed primarily of lymphocytes and plasma cells, with fewer macrophages. Electron microscopy revealed intracytoplasmic inclusions in endothelial cells (data not shown) and in hepatocytes (Fig. 7C). Immunoelectron microscopy confirmed that these inclusions were of hantavirus origin (Fig. 7D). In spite of the large size of some of these inclusions, endothelial cells and hepatocytes did not appear damaged. Moreover, blood chemistry analysis indicated normal liver function during the course of the experiment (Fig. 7E).

Pathology in other tissues. All other tissues from ANDV-injected hamsters, including the heart, thymus, trachea, thyroid gland, gastrointestinal tract, pancreas, kidneys, adrenal glands, urinary bladder, uterus, ovaries, skin, submandibular salivary gland, multiple lymph nodes, and multiple sections through the head, including brain, pituitary gland, eyes, and nasal turbinates, did not have lesions attributable to ANDV infection (data not shown). All tissues evaluated histologically in SNV-infected animals had no significant lesions attributed to viral infection. There were a variety of other lesions present in both the ANDV-infected hamsters and SNV-infected hamsters, all of which were considered age-related changes, background changes, or incidental findings.

DISCUSSION

Until recently, it had been impossible to perform temporal studies on the development of HPS because no animal model existed. Most of the studies investigating the pathogenesis of HPS involved the examination of postmortem tissue from hu-

(D) Type 1 epithelial cells in the lungs of animal 238 (day 12 postchallenge) were filled with edema fluid and detached from the basement membrane, which was also disrupted. Original magnification, ×67,500. (E) Ruffling of the apical surface of type 1 epithelial cells was frequently observed when edema fluid was present. This was observed as early as day 8 postchallenge, as shown in this representative image (animal 226). Original magnification, ×17,000. (F) Apoptotic lymphocytes were commonly observed in lung capillaries starting as early as day 4 postchallenge. Note the nuclear condensation that is a hallmark of apoptosis. Three apoptotic lymphocytes are seen in this pulmonary capillary from animal 207 (day 14 postchallenge). Original magnification, ×13,500X. RBC, red blood cell; MΦ, macrophage; Ly, lymphocyte; In, inclusion; Nu, nucleus; EC, endothelial cell; EpC, epithelial cell; BM, basement membrane.

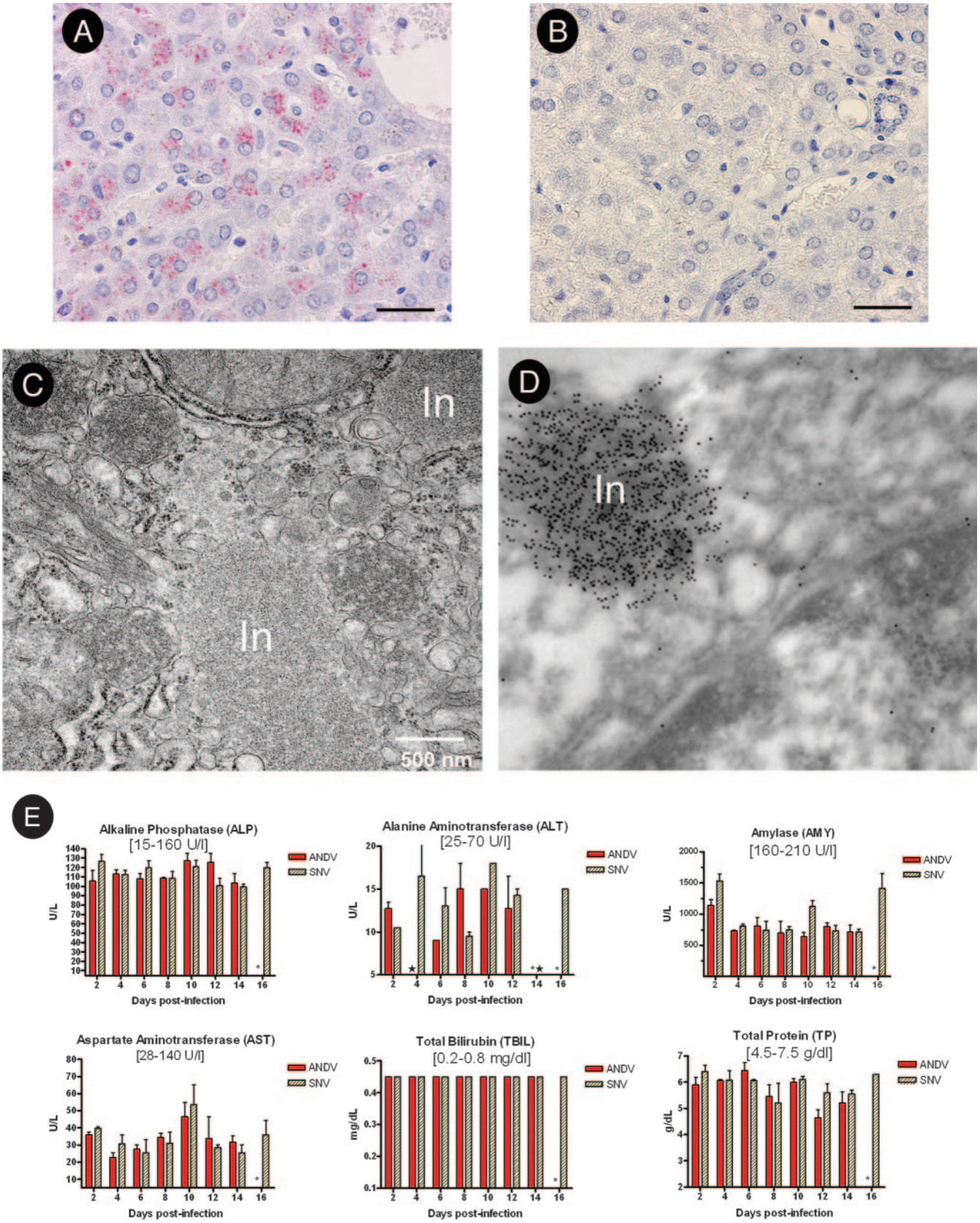

FIG. 7. Effects of hantavirus infection on the liver. An alkaline phosphatase immunohistochemical assay using anti-nucleocapsid antibody was performed on liver samples from ANDV-infected (animal 207) (A) or SNV-infected (animal 259) (B) animals at 14 days postinfection. For panels A and B, the bars represent 30 μm. (C) Ultrastructural analysis revealed large nucleocapsid inclusions within hepatocytes of the ANDV-infected

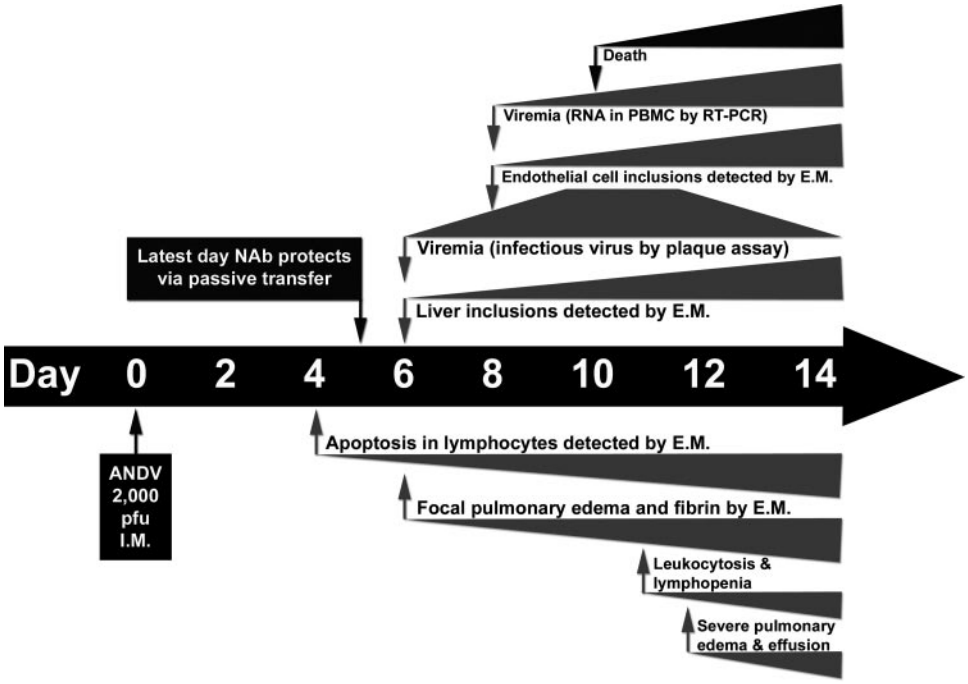

FIG. 8. Timeline of events during ANDV infection of hamsters. Hamsters were injected intramuscularly (i.m.) with 2,000 PFU of ANDV on day 0. On day 4, apoptosis of lymphocytes was first detected. Numbers of apoptotic lymphocytes increased with time, as illustrated by the expanding wedge. Day 5 is the last day that the passive transfer of neutralizing antibodies (Nabs) protected against lethal disease (21). By day 6, animals became viremic, inclusions became visible in the liver, and focal pulmonary edema was first detected. Endothelial cell inclusions were first detected on day 8, 1 day before the earliest deaths. During the late stages of infection, there was leukocytosis and lymphopenia and finally severe pulmonary edema and death. E.M., electron microscopy.

man HPS cases (43). The ANDV/hamster lethal HPS model has made it possible to perform temporal studies to follow the disease course from exposure to fulminant disease. This model was recently used to investigate the possibility that cardiogenic shock is involved in lethality of this disease (4). The authors used telemetry and found that the heart rate and blood pressure slowly dropped during the course of infection and that subsequently, during the 12 h preceding death, the blood pressure dropped rapidly and the heart rate increased by 20%. Here, we examined the pathogenesis of HPS as it evolved over time in the hamster and we compared the ANDV and SNV infections. We confirmed previous findings that ANDV, but not SNV, is lethal to the Syrian hamster. ANDV-infected hamsters lost up to 6% of their body weight during the 48 h preceding death. The mean time to death in this study was 11 days, and signs of disease were evident only during the final few hours before death or euthanasia. A summary of the days postchallenge when changes in the hamster were first observed is shown in Fig. 8. The earliest evidence of disease in ANDV-infected hamsters was apoptotic lymphocytes on day 4. Most of the changes, including infectious virus in the blood, viral inclusions in the liver, and focal pulmonary edema, were first observed on day 6. Earlier studies demonstrated that passive transfer of neutralizing antibodies on day 6 or later was not protective, whereas passive transfer on day 5 or earlier was protective (6).

Viremia. ANDV is highly lethal in hamsters, whereas SNV is not despite having a 50% infective dose of only 2 PFU (12). Here, we demonstrated that this strain difference correlates with virus dissemination. ANDV-infected hamsters developed viremia by day 6, as measured by infectious virus in whole blood or serum. Within 2 days, the level of infectious virus in the blood surpassed 10^7 PFU/ml, which is a titer similar to the maximal titer of ANDV obtained from Vero E6 cell culture supernatants. In contrast, infectious SNV was not detected in the whole blood or serum at any time point, and even RT-PCR assays failed to detect SNV genomes. We know that SNV replicated to levels sufficient to elicit a robust antibody response, and SNV antigen was detected by immunohistochemistry, albeit rarely, in endothelial cells of several organs on days 12 and 14 after challenge (Table 2). We hypothesize that following inoculum input, virus gained access to the blood and

hamsters. (D) Immunoelectron microscopy using anti-SNV nucleocapsid antibody confirmed that the inclusion bodies contained hantavirus antigen. Original magnification, ×80,000 (animal 227). (E) Serum chemistries from ANDV- and SNV-infected hamsters were determined using a general chemistry 12-disc panel rotor and a Piccolo point-of-care blood analyzer. Error bars represent the SEM. All bilirubin values were identical and within normal limits, as expected in the absence of significant liver damage. Normal reference ranges are shown in brackets. In, inclusion; *, no data; ⋆, below limit of detection.

spread to endothelial cells in various organs. Replication in those cells could evoke an adaptive immune response and could account for the sporadic antigen-positive cells detected at late time points by immunohistochemistry. Interestingly, staining was of single cells rather than foci, suggesting that viral spread, even to adjacent cells, was inhibited.

It remains unclear why ANDV was able to readily disseminate in the hamster while the closely related SNV did not. This could be due to differences in growth kinetics between these two viruses. In cell culture, ANDV grows to higher titers with faster kinetics than SNV (26). However, if a lag in SNV growth is responsible for the decreased virulence in hamsters, then we would expect to detect SNV viremia at a later time point (e.g., day 8 or 10), unless this lag delayed dissemination of SNV long enough for the adaptive immune response to neutralize the infection before dissemination could occur.

An alternative explanation for the absence of a SNV viremia could be innate immunity. It is possible that the innate immune system of hamsters rapidly recognized SNV as a threat and functioned to contain and suppress the infection. If this occurred, then ANDV must have somehow evaded the innate immune responses, either by passively replicating as an unrecognized threat or by actively disrupting innate immunity. Numerous viruses produce proteins that act as interferon antagonists or otherwise disrupt the innate immune system (2). ANDV was recently shown to interfere with interferon signaling in vitro (36). Research investigating the role of innate immunity in the differential outcome following infection of hamsters with SNV or ANDV is in progress.

Although viral nucleic acid is routinely detected in the blood and plasma of HPS patients by RT-PCR (38), infectious virus has never been isolated from an HPS patient. There is a single report describing the isolation of an HPS-associated hantavirus (ANDV) from an asymptomatic individual who later developed lethal HPS (8). High loads of viral nucleic acid in humans at hospital admission were associated with severe disease (41). In contrast, high SNV-neutralizing antibody titers at hospital admission were associated with a mild disease course (42). The inability to detect infectious virus in HPS patients could be due to neutralization of virus by the immune system before the onset of disease symptoms.

Lymphocyte apoptosis. The earliest pathology observed for ANDV-infected hamsters was the presence of apoptotic lymphocytes in lung capillaries starting on day 4 postchallenge as detected by electron microscopy. Apoptosis is an evolutionarily conserved and extremely ordered type of cell death that is important in regulating normal physiology and under certain circumstances plays a role in pathology (33). For example, during septic shock, patients exhibit absolute lymphocyte counts below the normal limits due to apoptosis (13). There have been several reports of in vitro studies that investigated if hantaviruses (largely HFRS associated) induce apoptosis in either Vero E6 cells (10, 15, 18–20), HEK293 cells (23), or peripheral blood lymphocytes (1). While some studies suggest that induction of apoptosis is replication dependent (15, 18), Markotic et al. suggest a bystander phenomenon (23). Zaki et al. did report the occasional presence of viral antigen within lymphocytes of humans infected with SNV (43). In our hamster model, lymphocyte apoptosis was detected early (2 days before viremia was detected). We did not observe the presence of viral inclusions within lymphocytes, suggesting a bystander mechanism. In hamsters infected with ANDV, early apoptosis of lymphocytes could result in immune dysfunction allowing dissemination of virus and subsequent fulminant disease. As hamster-specific reagents become available, it will become possible to test this hypothesis.

Vascular leakage. The primary abnormality in HFRS and HPS is vascular leakage. This leakage could be caused directly by interaction and/or infection of endothelial cells with hantaviruses, or indirectly by the immune response, or by a combination of direct and indirect effects on the cells. Direct interaction of pathogenic hantaviruses with $\alpha_v\beta_3$ integrins has been proposed as a possible mechanism of pathogenesis (22). The high level of viremia that we observed for the hamsters infected with ANDV allows the possibility that virus interaction with endothelial cell receptors, and not infection per se, could contribute to vascular leakage. It might be possible to test the effects of virus-cell interaction but not infection in vivo by infusion of high levels of inactivated virus, or pseudotyped virus, over a period of 2 or more days.

One of the hallmarks of in vitro hantavirus infection is the absence of cytolysis or marked cytopathic effect. However, this absence does not rule out the possibility that the cell functions have been disrupted. For example, infected Vero E6 cells do not take up neutral red in the same way uninfected cells do, and this difference is the basis for the hantavirus plaque assay. Our electron microscopy data confirm earlier H&E observations that cytolyis and necrosis are not occurring in the endothelial cells of ANDV-infected hamsters. Ultrastructural analysis did not reveal gaps between adjacent endothelial cells, suggesting that paracellular permeability was not the mechanism of leakage. However, the possibility that undetected transient formation of gaps between cells might occur cannot be ruled out. Interestingly, we observed increased numbers of vacuoles in the endothelial cells of infected tissue (Fig. 5B). Many of these cells contained viral inclusions, suggesting that the mechanism of leakage might involve transcellular transport of fluid through productively infected cells. If transcellular transport of plasma across endothelial cells were to occur, the fluid might affect the basement membrane and epithelial cells that form the barrier between the capillary lumen and alveolar space. Supporting this, we observed the presence of edema in lung epithelial cells, and in some cases the basement membrane appeared diffuse and possibly disrupted (Fig. 5D and E). It is remarkable that these were the only ultrastructural abnormalities observed despite the fact that very high volumes of fluid crossed from the lung capillaries into the alveolar spaces and pleural cavity.

Despite some evidence for a direct role of hantavirus infection on endothelial cell leakage, there are several lines of evidence indicating that the immune response plays a role in the pathogenesis. For example, we observed large numbers of mononuclear cell infiltrates within the alveoli and in the perivascular interstitium. It is possible that the cytokines released by these cells caused the vascular leakage. Indeed, there are some compelling data in the hantavirus literature to support this theory. Immunohistological analysis of kidney biopsies taken during the acute phase of HFRS caused by Puumala virus revealed an increase in levels of local cytokines including tumor necrosis factor alpha (TNF-α), platelet-derived growth

factor, and transforming growth factor beta (37). In the same study, increased expression levels of ICAM-1, VCAM-1, and PECAM were also seen in the same sites of the peritubular area of distal nephrons. Systemic levels of inflammatory cytokines have also been reported for plasma of HFRS patients and include TNF-α, soluble TNF-α receptor, interleukin-6 (IL-6), and IL-10 (21). The increased levels of TNF-α seen in HFRS may have a profound impact both locally and systemically on vascular integrity. TNF-α, along with other proinflammatory mediators, is known to cause reduced hepatic, renal, pulmonary, and/or cardiac functions during septic shock and viral hemorrhagic fever infection caused by filoviruses (3). Elevated levels of TNF-α are capable of altering endothelial cell junctions, actin stress fibers, and ultimately vascular permeability (7, 40). Many of the symptoms seen during hantavirus infection in humans, including fever, chills, myalgia, hypotension, and edema formation, are reminiscent of septic shock. Increased levels of proinflammatory mediators during hantavirus infection are not limited to HFRS. Mori et al. described increased production of vasoactive cytokines (IL-1α, IL-1β, IL-6, and TNF-α) throughout the lung tissue of HPS patients (27). Gamma interferon and IL-2 were also detected in the lungs of HPS patients, and gamma interferon from activated T cells may act to exacerbate shock in vivo (27). Finally, a genetic predisposition to high-level production of TNF-α through the TNF2 allele was observed more frequently for hospitalized HFRS cases than for normal controls (14). As reagents for measuring hamster cytokines and chemokines become available, it will be possible to determine what role(s), if any, proinflammatory and/or anti-inflammatory responses play in the HPS caused by ANDV in hamsters.

Concluding remarks. Previous studies by our laboratory have shown that the latest time point that passive transfer of neutralizing antibodies will protect against a lethal ANDV challenge is day 5 postinfection (6). In this study, we observed that ANDV-infected hamsters were viremic by day 6 postinfection, an observation that may explain the lack of efficacy for passive transfer of neutralizing antibodies at later times. Pathology in the lung was first observed at day 8 postinfection, shortly after the viremia. We suspect that ANDV replicated at low levels during the first 5 days of infection and then rapidly burst from the initial infection site and spread to multiple organs, likely by seeding endothelial cells that were uniformly infected. Massive nucleocapsid inclusions were observed for endothelial cells of all organs examined; however, endothelial cell architecture was largely unaffected. Furthermore, these inclusions were observed for hepatocytes and interestingly did not alter the ability of these cells to function, as measured by blood chemistry analysis (Fig. 7). Taken together, these data suggest that hantavirus countermeasures aimed at preventing virus replication and dissemination will have the greatest probability of success if administered within the first 5 days postexposure (before the viremic phase). Nevertheless, our data suggest that because vascular leakage appears to be associated with infected endothelial cells, a therapeutic strategy targeting viral replication might be effective in treating this disease even at later times. This is important because most HPS patients are first identified upon admission to the emergency room after disease onset. In the present study, we identified previously unrecognized similarities between the hamster model and HPS in humans, including lymphopenia, neutrophilia, mild thrombocytopenia, and lymphocyte apoptosis. The hamster model will be an important system for testing the effectiveness of candidate antiviral modalities administered at early and late times in the disease course.

ACKNOWLEDGMENTS

We gratefully acknowledge C. Mech for her work on immunohistochemistry and G. Krietz, J. Brubaker, N. Davis, S. Moon, K. Kuehl, and J. Smith for excellent technical assistance. All experiments involving the use of ANDV or SNV in animals were performed in USAMRIID's BSL-4 laboratory, and all other work involving infectious hantaviruses were performed in a BSL-3 laboratory at USAMRIID. Research was conducted in compliance with the Animal Welfare Act and other federal statutes and regulations relating to animals and experiments involving animals and adheres to principles stated in the *Guide for the Care and Use of Laboratory Animals*, National Research Council, 1996 (27a). The facility where this research was conducted is fully accredited by the Association for Assessment and Accreditation of Laboratory Animal Care International.

The research described herein was sponsored by the Military Infectious Disease Research Program, U.S. Army Medical and Material Command, project no. AT0002_04_RD. This research was performed while V. Wahl-Jensen and R. Fisher held National Research Council Research Associateship Awards at USAMRIID.

Opinions, interpretations, conclusions, and recommendations are ours and are not necessarily endorsed by the U.S. Army or the Department of Defense.

REFERENCES

1. **Akhmatova, N. K., R. S. Yusupova, S. F. Khaiboullina, and S. V. Sibiryak.** 2003. Lymphocyte apoptosis during hemorragic fever with renal syndrome. Russ. J. Immunol. **8:**37–46.
2. **Basler, C. F., and A. Garcia-Sastre.** 2002. Viruses and the type I interferon antiviral system: induction and evasion. Int. Rev. Immunol. **21:**305–337.
3. **Bray, M., and S. Mahanty.** 2003. Ebola hemorrhagic fever and septic shock. J. Infect. Dis. **188:**1613–1617.
4. **Campen, M. J., M. L. Milazzo, C. F. Fulhorst, C. J. Obot Akata, and F. Koster.** 2006. Characterization of shock in a hamster model of hantavirus infection. Virology **356:**45–49.
5. **Centers for Disease Control and Prevention.** 2006. Hantavirus pulmonary syndrome–five states, 2006. Morb. Mortal. Wkly. Rep. **55:**627–629.
6. **Custer, D. M., E. Thompson, C. S. Schmaljohn, T. G. Ksiazek, and J. W. Hooper.** 2003. Active and passive vaccination against hantavirus pulmonary syndrome with Andes virus M genome segment-based DNA vaccine. J. Virol. **77:**9894–9905.
7. **Feldmann, H., H. Bugany, F. Mahner, H. D. Klenk, D. Drenckhahn, and H. J. Schnittler.** 1996. Filovirus-induced endothelial leakage triggered by infected monocytes/macrophages. J. Virol. **70:**2208–2214.
8. **Galeno, H., J. Mora, E. Villagra, J. Fernandez, J. Hernandez, G. J. Mertz, and E. Ramirez.** 2002. First human isolate of Hantavirus (Andes virus) in the Americas. Emerg. Infect. Dis. **8:**657–661.
9. **Goldsmith, C. S., L. H. Elliott, C. J. Peters, and S. R. Zaki.** 1995. Ultrastructural characteristics of Sin Nombre virus, causative agent of hantavirus pulmonary syndrome. Arch. Virol. **140:**2107–2122.
10. **Hardestam, J., J. Klingstrom, K. Mattsson, and A. Lundkvist.** 2005. HFRS causing hantaviruses do not induce apoptosis in confluent Vero E6 and A-549 cells. J. Med. Virol. **76:**234–240.
11. **Hooper, J. W., K. I. Kamrud, F. Elgh, D. Custer, and C. S. Schmaljohn.** 1999. DNA vaccination with hantavirus M segment elicits neutralizing antibodies and protects against Seoul virus infection. Virology **255:**269–278.
12. **Hooper, J. W., T. Larsen, D. M. Custer, and C. S. Schmaljohn.** 2001. A lethal disease model for hantavirus pulmonary syndrome. Virology **289:**6–14.
13. **Hotchkiss, R. S., P. E. Swanson, B. D. Freeman, K. W. Tinsley, J. P. Cobb, G. M. Matuschak, T. G. Buchman, and I. E. Karl.** 1999. Apoptotic cell death in patients with sepsis, shock, and multiple organ dysfunction. Crit. Care Med. **27:**1230–1251.
14. **Kanerva, M., A. Vaheri, J. Mustonen, and J. Partanen.** 1998. High-producer allele of tumour necrosis factor-alpha is part of the susceptibility MHC haplotype in severe puumala virus-induced nephropathia epidemica. Scand. J. Infect. Dis. **30:**532–534.
15. **Kang, J. I., S. H. Park, P. W. Lee, and B. Y. Ahn.** 1999. Apoptosis is induced by hantaviruses in cultured cells. Virology **264:**99–105.
16. **Lee, J. S., J. Lahdevirta, F. Koster, and H. Levy.** 1999. Clinical manifestations and treatment of HFRS and HPS, p. 17–38. *In* H. W. Lee, C. Calisher, and C. Schmaljohn (ed.), Manual of hemorrhagic fever with renal syndrome

and hantavirus pulmonary syndrome. ASAN Institute for Life Sciences, Seoul, Korea.
17. **Levis, S., J. E. Rowe, S. Morzunov, D. A. Enria, and S. St Jeor.** 1997. New hantaviruses causing hantavirus pulmonary syndrome in central Argentina. Lancet **349:**998–999.
18. **Li, X. D., S. Kukkonen, O. Vapalahti, A. Plyusnin, H. Lankinen, and A. Vaheri.** 2004. Tula hantavirus infection of Vero E6 cells induces apoptosis involving caspase 8 activation. J. Gen. Virol. **85:**3261–3268.
19. **Li, X. D., H. Lankinen, N. Putkuri, O. Vapalahti, and A. Vaheri.** 2005. Tula hantavirus triggers pro-apoptotic signals of ER stress in Vero E6 cells. Virology **333:**180–189.
20. **Li, X. D., T. P. Makela, D. Guo, R. Soliymani, V. Koistinen, O. Vapalahti, A. Vaheri, and H. Lankinen.** 2002. Hantavirus nucleocapsid protein interacts with the Fas-mediated apoptosis enhancer Daxx. J. Gen. Virol. **83:**759–766.
21. **Linderholm, M., C. Ahlm, B. Settergren, A. Waage, and A. Tarnvik.** 1996. Elevated plasma levels of tumor necrosis factor (TNF)-alpha, soluble TNF receptors, interleukin (IL)-6, and IL-10 in patients with hemorrhagic fever with renal syndrome. J. Infect. Dis. **173:**38–43.
22. **Mackow, E. R., and I. N. Gavrilovskaya.** 2001. Cellular receptors and hantavirus pathogenesis. Curr. Top. Microbiol. Immunol. **256:**91–115.
23. **Markotic, A., L. Hensley, T. Geisbert, K. Spik, and C. Schmaljohn.** 2003. Hantaviruses induce cytopathic effects and apoptosis in continuous human embryonic kidney cells. J. Gen. Virol. **84:**2197–2202.
24. **Martinez, V. P., C. Bellomo, J. San Juan, D. Pinna, R. Forlenza, M. Elder, and P. J. Padula.** 2005. Person-to-person transmission of Andes virus. Emerg. Infect. Dis. **11:**1848–1853.
25. **McElroy, A. K., M. Bray, D. S. Reed, and C. S. Schmaljohn.** 2002. Andes virus infection of cynomolgus macaques. J. Infect. Dis. **186:**1706–1712.
26. **McElroy, A. K., J. M. Smith, J. W. Hooper, and C. S. Schmaljohn.** 2004. Andes virus M genome segment is not sufficient to confer the virulence associated with Andes virus in Syrian hamsters. Virology **326:**130–139.
27. **Mori, M., A. L. Rothman, I. Kurane, J. M. Montoya, K. B. Nolte, J. E. Norman, D. C. Waite, F. T. Koster, and F. A. Ennis.** 1999. High levels of cytokine-producing cells in the lung tissues of patients with fatal hantavirus pulmonary syndrome. J. Infect. Dis. **179:**295–302.
27a. **National Research Council.** 1996. Guide for the care and use of laboratory animals. National Academy Press, Washington, DC.
28. **Nichol, S. T.** 2001. Bunyaviruses, p. 1603. *In* D. M. Knipe, P. M. Howley, and D. E. Griffin, R. A. Lamb, M. A. Martin, B. Roizman, and S. E. Straus (ed.), Fields virology, 4th ed., vol. 1. Lippincott Williams & Wilkins, Philadelphia, PA.
29. **PAHO.** 2004. Number of cases of hantavirus pulmonary syndrome (HPS) (region of the Americas, 1993–2004). http://www.paho.org/common/Display.asp?Lang=E&RecID=1971.
30. **Pinna, D. M., V. P. Martinez, C. M. Bellomo, C. Lopez, and P. Padula.** 2004. New epidemiologic and molecular evidence of person to person transmission of hantavirus Andes Sout. Medicina (Buenos Aires) **64:**43–46. (In Spanish.)
31. **ProMED-mail.** 2006. Hantavirus pulmonary syndrome-Canada ex Bolivia. http://www.promedmail.org/pls/promed/f?p=2400:1001:9753834909080299352::NO::F2400_P1001_BACK_PAGE,F2400_P1001_PUB_MAIL_ID:1010,33838.
32. **Prophet, E. B., B. Mills, J. B. Arrington, and L. H. Sobin.** 1992. Laboratory methods for histotechnology. Armed Forces Institute of Pathology, Washington, DC.
33. **Raff, M.** 1998. Cell suicide for beginners. Nature **396:**119–122.
34. **Schmaljohn, A. L., D. Li, D. L. Negley, D. S. Bressler, M. J. Turell, G. W. Korch, M. S. Ascher, and C. S. Schmaljohn.** 1995. Isolation and initial characterization of a newfound hantavirus from California. Virology **206:**963–972.
35. **Schmaljohn, C., and J. W. Hooper.** 2001. Bunyaviridae: the viruses and their replication, p. 1581–1602. *In* B. N. Fields, D. M. Knipe, and P. M. Howley (ed.), Field's virology. Lippincott-Raven, Philadelphia, PA.
36. **Spiropoulou, C. F., C. G. Albarino, T. G. Ksiazek, and P. E. Rollin.** 2007. Andes and Prospect Hill hantaviruses differ in early induction of interferon although both can down-regulate interferon signaling. J. Virol. **81:**2769–2776.
37. **Temonen, M., J. Mustonen, H. Helin, A. Pasternack, A. Vaheri, and H. Holthofer.** 1996. Cytokines, adhesion molecules, and cellular infiltration in nephropathia epidemica kidneys: an immunohistochemical study. Clin. Immunol. Immunopathol. **78:**47–55.
38. **Terajima, M., J. D. Hendershot III, H. Kariwa, F. T. Koster, B. Hjelle, D. Goade, M. C. DeFronzo, and F. A. Ennis.** 1999. High levels of viremia in patients with the hantavirus pulmonary syndrome. J. Infect. Dis. **180:**2030–2034.
39. **Tischler, N. D., H. Galeno, M. Rosemblatt, and P. D. Valenzuela.** 2005. Human and rodent humoral immune responses to Andes virus structural proteins. Virology **334:**319–326.
40. **Wahl-Jensen, V. M., T. A. Afanasieva, J. Seebach, U. Stroher, H. Feldmann, and H. J. Schnittler.** 2005. Effects of Ebola virus glycoproteins on endothelial cell activation and barrier function. J. Virol. **79:**10442–10450.
41. **Xiao, R., S. Yang, F. Koster, C. Ye, C. Stidley, and B. Hjelle.** 2006. Sin Nombre viral RNA load in patients with hantavirus cardiopulmonary syndrome. J. Infect. Dis. **194:**1403–1409.
42. **Ye, C., J. Prescott, R. Nofchissey, D. Goade, and B. Hjelle.** 2004. Neutralizing antibodies and Sin Nombre virus RNA after recovery from hantavirus cardiopulmonary syndrome. Emerg. Infect. Dis. **10:**478–482.
43. **Zaki, S. R., P. W. Greer, L. M. Coffield, C. S. Goldsmith, K. B. Nolte, K. Foucar, R. M. Feddersen, R. E. Zumwalt, G. L. Miller, A. S. Khan, et al.** 1995. Hantavirus pulmonary syndrome. Pathogenesis of an emerging infectious disease. Am. J. Pathol. **146:**552–579.
44. **Zaki, S. R., and K. B. Nolte.** 1999. Pathology, immunohistochemistry and in situ hybridization, p. 143–154. *In* H. W. Lee, C. E. Calisher, and C. Schmaljohn (ed.), Manual of hemorrhagic fever with renal syndrome and hantavirus pulmonary syndrome. ASAN Institute for Life Sciences, Seoul, Korea.